Eur. Phys. J. B **14**, 83–90 (2000)

THE EUROPEAN PHYSICAL JOURNAL B

EDP Sciences

On the 240 K anomaly in the magnetic properties of $LiNiO_2$

F. Reynaud[1], A.M. Ghorayeb[1,a], Y. Ksari[1], N. Menguy[1], A. Stepanov[1], and C. Delmas[2]

[1] Laboratoire MATériaux: Organisation et Propriétés, CNRS, Case 151, Faculté des Sciences de Saint-Jérôme, Université d'Aix-Marseille III, 13397 Marseille Cedex 20, France

[2] Institut de Chimie de la Matière Condensée de Bordeaux, CNRS, École Nationale Supérieure de Chimie et Physique de Bordeaux, 87 avenue du Docteur Albert Schweitzer, 33608 Pessac Cedex, France

Received 14 May 1999 and Received in final form 5 August 1999

Abstract. In this work, results of X-band ESR spectroscopy, ac-magnetic susceptibility and X-ray powder diffraction measurements on $Li_{1-x}Ni_{1+x}O_2$ ($x = 0.02$ and $x = 0.07$) are presented and discussed. While the susceptibility of the compound with $x = 0.02$ is shown to follow a Curie-Weiss law, with a Weiss temperature of the order of 30 K, the compound with $x = 0.07$ is found to order ferromagnetically below ~ 80 K. However, an additional anomaly is observed in the magnetic properties of this latter compound at around 240 K. We attribute this anomaly to the presence of macroscopic Ni-rich regions which order ferrimagnetically below this temperature. This phenomenon is different from the bulk ferromagnetism that occurs at much lower temperatures, and allows us to discard earlier suggestions proposed in the literature in which the 240 K anomaly has been considered as denoting an intrinsic phenomenon.

PACS. 76.30.-v Electron paramagnetic resonance and relaxation – 76.50.+g Ferromagnetic, antiferromagnetic, and ferrimagnetic resonances; spin-wave resonance – 75.30.Et Exchange and superexchange interactions

1 Introduction

Although first reported in the late fifties [1], the layered-structure oxide $LiNiO_2$ continues to be the subject of considerable interest, both from the fundamental and the applied aspects of solid state research. The ideal crystal structure of this compound is rhombohedral ($R\bar{3}m$ space group) and is built up of an alternation of lithium layers and NiO_2 slabs made up of edge-sharing NiO_6 octahedra, the lithium ions also being in octahedral coordination (see Fig. 1a). The smallest Ni-Ni distance within an NiO_2 slab (2.88 Å) is much shorter than that between two adjacent slabs (4.73 Å), giving this compound a two-dimensional (2D) character. However, synthesizing stoichiometric $LiNiO_2$ has so far been unsuccessful. In fact, there are always some extra Ni ions occupying Li sites [2], so that the real chemical formula should be expressed as $Li_{1-x}Ni_{1+x}O_2$. The presence of these extra Ni ions in the Li layers has given rise to many questions. On the side of industrial applications, while the two-dimensional nature of $LiNiO_2$ makes this compound suitable for use as an electrode in high energy density batteries [3–6], the extra Ni ions hinder the diffusion of Li in between the NiO_2 slabs and, thereby, reduce the efficiency of these batteries. On the other hand, the magnetic properties of $Li_{1-x}Ni_{1+x}O_2$ are strongly dependent on the concentration, x, of extra Ni ions and have been the subject of numerous studies with often contradictory results, particularly at low temperatures where, for small values of x, this compound has been described as a ferrimagnet below 241 K [1], a triangular lattice spin-1/2 antiferromagnet with a quantum spin liquid ground state [7–11], a weakly coupled 2D Ising ferromagnet [12,13], a ferromagnet without spontaneous magnetization at low temperatures [14–16], a spin glass [2,17–20] or a frustrated system with the presence of ferrimagnetic clusters [21] evolving into 3D ferrimagnetism below 240 K for $x > 0.24$. In fact, at this temperature of 240 K, anomalies in the magnetic properties of $LiNiO_2$ have been reported by various authors with a different interpretation in each case. Hirota and co-workers [22,23] have deduced from dc susceptibility, resistivity and specific heat measurements that $LiNiO_2$ is a Curie-Weiss paramagnet above 240 K and enters, at that temperature, a frustrated spin state of planar short range order on the triangular lattice, down to ~ 70 K where inter-planar correlations start growing, until a frozen spin state is reached below ~ 35 K. Yoshizawa and co-workers [24] performed small-angle neutron scattering measurements on this compound and found ferromagnetic short-range spin correlations below 240 K, which were confirmed later by Reimers *et al.* [2] from magnetic susceptibility measurements and attributed to inter-layer Ni-Ni interactions. SQUID magnetometry studies by Yamaura *et al.* [19] revealed an anomaly around 240 K in the low-field magnetization curve, which was

[a] e-mail: ghorayeb@matop.u-3mrs.fr

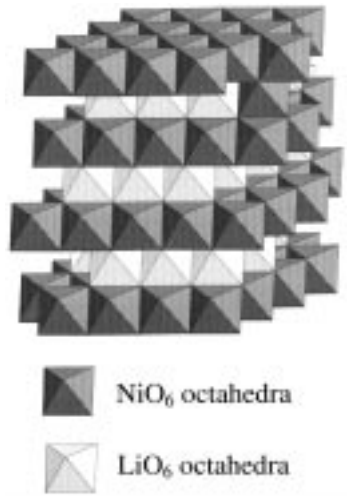

(a)

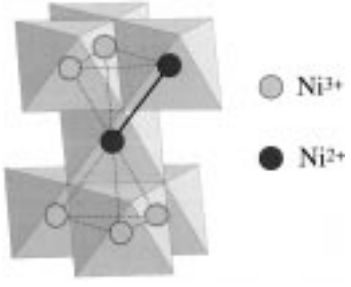

(b)

Fig. 1. (a) A perspective view of the crystal structure of $Li_{1-x}Ni_{1+x}O_2$ showing NiO_2 slabs alternating with lithium planes. One extra Ni ion is represented in one of the Li planes; (b) A seven-nickel ion cluster. The oxygen octahedra are also shown.

attributed to the possible presence of a small amount of impurity phase of low Li content resulting either from insufficient reactivity during the growth phase or from thermal loss of Li at high temperatures. More recently, some of us [25] reported preliminary high magnetic field spin resonance results on nearly stoichiometric $LiNiO_2$ (particularly on samples with $x = 0.02$ and $x = 0.06$) and found that, while the $x = 0.02$ sample remained paramagnetic down to low temperatures, the sample with $x = 0.06$ showed additional ferromagnetic-like signals below 240 K, indicative of ferromagnetic cluster resonance.

In this paper, we present magnetic susceptibility, X-band electron spin resonance (ESR) and X-ray powder diffraction measurements on samples of $Li_{1-x}Ni_{1+x}O_2$ with $x = 0.02$ and $x = 0.07$ in order to further investigate the possible origin of this 240 K anomaly which has so far been the subject of various interpretations in the literature.

2 Experimental considerations

Powder samples of $Li_{1-x}Ni_{1+x}O_2$ (with $x = 0.02$ and $x = 0.07$) have been prepared following the procedure described by Rougier *et al.* [26].

X-ray diffraction experiments have been performed on these samples, and data were obtained using a Philips X'Pert MPD powder diffractometer equipped with a PW3050 theta-theta goniometer and a Cu-Kα diffracted beam graphite monochromator. Patterns were collected in the angular range $15° < 2\theta < 120°$ in step scan mode with a step of 0.01° and 30 s of counting time. Parallel (Soller) slits with a 0.02 rad aperture were used in order to limit the axial divergence. A fixed divergence slit of 0.25° and a receiving slit of 0.2 mm were also used.

The ESR measurements were performed on a BRUKER EMX spectrometer operating in the X-band ($\nu = 9.45$ GHz). The static magnetic field was scanned from 0.005 T to 0.905 T and the modulation field used had an amplitude of 0.002 T and a frequency of 100 kHz. The spectrometer was adapted for low temperature measurements using a controlled nitrogen flow, and spectra could be recorded at various temperatures in the range 95 K–300 K, the temperature being stabilized to within 0.5 K in each case.

The ac-susceptibility measurements as a function of temperature were performed on an Oxford Instruments MAGLAB system^{2000} equipped with a superconducting coil allowing measurements to be made in the presence of a static magnetic field of up to 7 T if needed. The samples, which had a typical mass of about 50 mg, were placed in thin Pyrex tubes. The measurements were made using an ac field of 3×10^{-4} T at 10 kHz, in the absence of any external field. However, in addition, the susceptibility of the $Li_{0.93}Ni_{1.07}O_2$ compound was also measured in the presence of a dc field of 2 T. The temperature was regulated using an Oxford Instruments ITC^{503} controller. During the measurements, the temperature was varied at a rate of 0.2 Kmin^{-1}. In view of the question addressed in this work, the study as a function of temperature was restricted to the temperature range 100 K–300 K.

3 Results

3.1 ESR measurements

In Figure 2 we show the evolution of the ESR spectra of $Li_{0.98}Ni_{1.02}O_2$ as a function of temperature between 100 K and room temperature.

The ordinate axis represents the derivative of absorption with respect to magnetic field, dA/dH. For the sake of clarity, the curves recorded at the indicated temperatures have been here rescaled so as to have the same peak-to-peak amplitude, and have been slightly shifted with respect to one another along the ordinate axis. From these results we may notice the following: firstly, the signal is fairly symmetric around the resonance field, H_r,

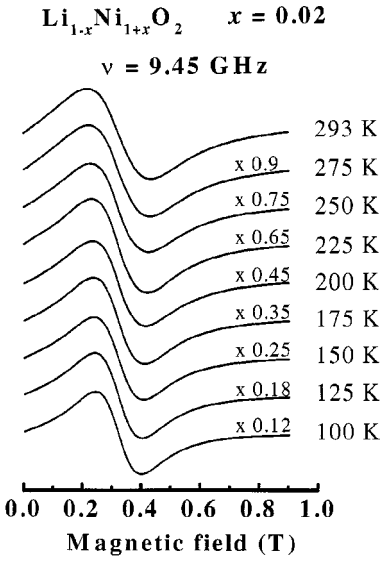

Fig. 2. The evolution with temperature of the ESR spectra of a typical sample of $Li_{0.98}Ni_{1.02}O_2$ between 100 K and room temperature. For the sake of clarity, the curves have been rescaled so as to have the same peak-to-peak amplitude, and have been slightly shifted with respect to one another along the ordinate axis. The number indicated on each curve represents the factor by which the corresponding curve has been multiplied in order to have the same amplitude as the room-temperature curve.

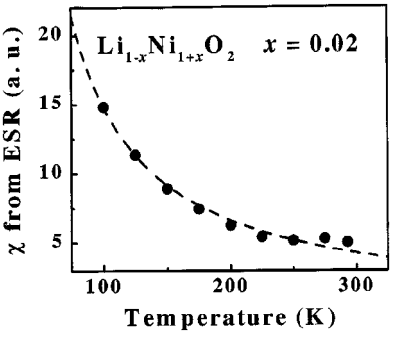

Fig. 3. The spin susceptibility of $Li_{0.98}Ni_{1.02}O_2$ as deduced from the integral of the ESR absorption intensity (filled circles) and a Curie-Weiss law fit to the data (dashed curve).

and remains so throughout the temperature range studied, indicating that it may reasonably be attributed to a single type of species. Indeed, it was possible to fit the spectra with a single Lorentzian function, giving an H_r value of 0.328 T at 300 K (which hardly varies with temperature ($\Delta H_r/H_r < 3\%$)), implying a g-factor of 2.06. Secondly, no sign of any anisotropy appears in the signal, despite the fact that the compound studied is anisotropic. Thirdly, the absorption increases with decreasing temperature, such that the integral of this absorption over the magnetic field range studied, which, in fact, is proportional to the spin susceptibility χ follows a Curie-Weiss law as is shown in Figure 3.

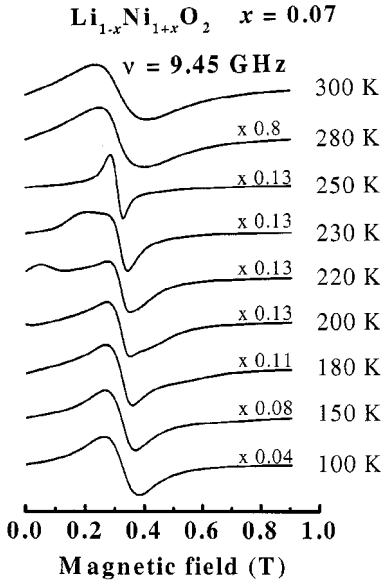

Fig. 4. The evolution with temperature of the ESR spectra of a typical sample of $Li_{0.93}Ni_{1.07}O_2$ between 100 K and 300 K. As in Figure 2, the curves have been rescaled and slightly shifted with respect to one another along the ordinate axis.

It is clear from this figure that the Curie-Weiss law, $\chi = C/(T - \theta)$, is reasonably well obeyed, with a characteristic temperature, θ, of 19 K as deduced from the fit. We shall discuss all the above mentioned results later in this paper.

We now show in Figure 4 the evolution with temperature, between 100 K and 300 K, of the ESR spectra corresponding to $Li_{0.93}Ni_{1.07}O_2$. As in Figure 2, the curves have been rescaled and shifted for clarity.

Important differences may be noted between these results on the $x = 0.07$ sample and those shown in Figure 2 on the sample with $x = 0.02$. In the temperature range 300 K to 250 K, while the spectra apparently still show a single resonance signal, the increase in absorption intensity with decreasing temperature is much more marked here than in the case of $Li_{0.98}Ni_{1.02}O_2$. This indicates that a second signal is superimposed on the first one in this temperature range proving the presence of another phase in the sample. Indeed, fitting these spectra with a single Lorentzian function proved unsuccessful, whereas considering the sum of two Lorentzian functions gave a much better fit to the data, indicating two resonance fields, H_{r1} and H_{r2}, one of which (H_{r1}) being equal to 0.331 T (giving a g-factor of 2.04) and the other (H_{r2}) being 0.311 T (implying a g-factor of 2.17). Below 250 K, it may be seen from Figure 4 that, while one signal remains centered around the same field value (H_{r1}), the second signal gives way to two distinct features appearing on either side of the central signal. Furthermore, the low-field feature shifts to lower field values as the temperature decreases, while the higher-field one shifts to higher field values.

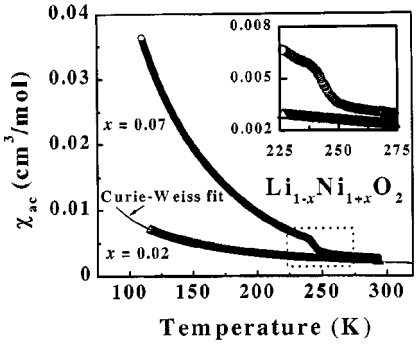

Fig. 5. Temperature variation of the ac susceptibility of $Li_{1-x}Ni_{1+x}O_2$ with $x = 0.02$ and $x = 0.07$. A Curie-Weiss fit to the data of the sample with $x = 0.02$ is also shown. The insert gives an enlarged view of the anomaly observed at 240 K in the susceptibility of the $x = 0.07$ sample and, at the same time, shows the absence of such an anomaly in the case of the sample with $x = 0.02$.

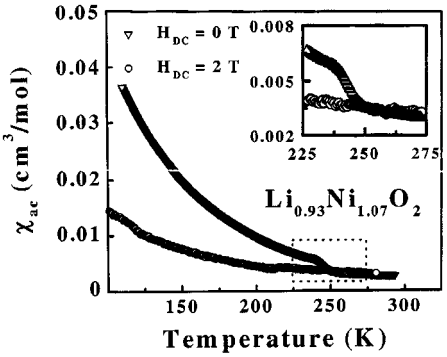

Fig. 6. Temperature variation of the ac susceptibility of $Li_{0.93}Ni_{1.07}O_2$, measured in the absence (triangles) and in the presence (circles) of an external magnetic field of 2 T. The insert gives an enlarged view of the part of the curves corresponding to the temperature range 225 K–275 K.

3.2 Magnetic susceptibility measurements

The variation with temperature of the ac magnetic susceptibility, χ_{ac}, of $Li_{1-x}Ni_{1+x}O_2$, with no external magnetic field applied, is shown in Figure 5 for the samples with $x = 0.02$ and $x = 0.07$, from room temperature down to 115 K.

One of the conclusions that we may deduce from these results is that the susceptibility of the sample with $x = 0.02$ follows a Curie-Weiss law, $\chi_{ac} = C/(T - \theta)$, with $C = 0.6$ cm^{3}Kmol^{-1} and $\theta \approx 34$ K. The discrepancy between this value of θ and that deduced from the ESR data (*cf.* Fig. 3) is not surprising since the temperature range over which the Curie-Weiss fit is performed is, in either case, not considerably large. Another important result that may be seen in Figure 5 is that, for the sample with $x = 0.07$, a clear anomaly occurs around 240 K in the χ_{ac} - *vs.* - temperature curve. Besides, for temperatures higher than 240 K, a Curie-Weiss fit to the data gives a θ value of the order of 80 K, whereas below 240 K, the susceptibility shows an important increase which is rather exponential. In order to try to understand the origin of this anomaly, we have performed susceptibility measurements with the sample being in the presence of an external magnetic field of 2 T. A comparison between the two curves, corresponding to the cases with and without applied magnetic field, is given here in Figure 6.

We may note from this figure that the application of an external magnetic field of 2 T suppresses the 240 K anomaly which was present in the susceptibility curve when no magnetic field was applied.

3.3 X-ray powder diffraction measurements

The X-ray diffraction results obtained on both of the compounds studied indicate that the positions of the peaks are compatible with the $R\bar{3}m$ space group over the whole

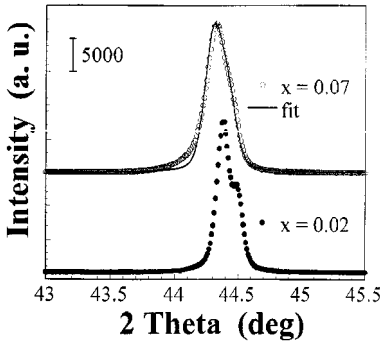

Fig. 7. The 104 diffraction peak for $Li_{1-x}Ni_{1+x}O_2$ with $x = 0.02$ and $x = 0.07$. For $x = 0.02$, only the Cu-Kα doublet is observed. For $x = 0.07$, a clearly visible asymmetry on the low angle side of the peak (revealed by the attempted fit; see text for details) as well as an important broadening are observed.

diffraction pattern. Nevertheless, for the $Li_{0.93}Ni_{1.07}O_2$ compound, a careful examination of the diffraction pattern reveals the presence of an unusual asymmetric shape for the diffraction peaks. For instance, Figure 7 shows a comparison between the shape of the 104 peak (which is not split off in the $R\bar{3}m$ space group symmetry) for $Li_{1-x}Ni_{1+x}O_2$ with $x = 0.07$ and $x = 0.02$.

For the $Li_{0.98}Ni_{1.02}O_2$ compound, the Kα doublet is observed whereas a significant broadening and a clearly visible asymmetric shape may be noted on the low angle side of the peak for the $Li_{0.93}Ni_{1.07}O_2$ compound. In the concerned angular range of Figure 7, such an asymmetry cannot be explained by the "umbrella" effect usually observed at low angle for powder diffraction patterns. Moreover, as the two X-ray powder diffraction experiments have been performed in the same conditions, the comparison shows that the asymmetric shape is due to a particular structural feature of the $Li_{0.93}Ni_{1.07}O_2$ compound.

As shown in Figure 7, an attempt to fit the 104 peak related to the $Li_{0.93}Ni_{1.07}O_2$ compound using two pseudo-Voigt functions for the Cu-Kα doublet was unsuccessful.

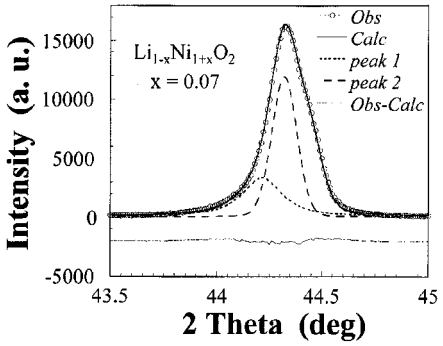

Fig. 8. A fit of the 104 diffraction peak for the $Li_{0.93}Ni_{1.07}O_2$ compound performed using two sets of pseudo-Voigt functions.

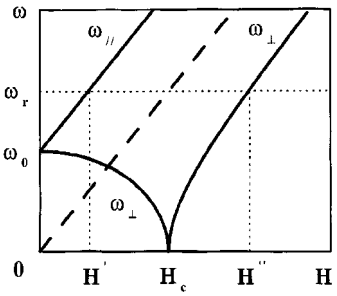

Fig. 9. Theoretical variation of the spin precession frequency ω as a function of applied magnetic field. The dashed curve corresponds to the case of a paramagnet. The full curves represent the case of a ferromagnet: $\omega_{\parallel}$ ($\omega_{\perp}$) is relative to the case where the applied field is parallel (perpendicular) to the easy axis of magnetization.

Figure 8 shows a fit of the 104 diffraction peak performed using two sets of pseudo-Voigt functions for the $Li_{0.93}Ni_{1.07}O_2$ compound. It may be easily seen that the two-component fit is better than the single-component one shown in Figure 7. This fact leads us to assume the coexistence of two phases in our $Li_{0.93}Ni_{1.07}O_2$ compound, and is in line with the deduction obtained from the ESR data presented in Section 3.1.

4 Discussion

In the light of the results presented above, we may deduce the following. While the ESR and ac-susceptibility measurements confirm the paramagnetic character of $Li_{1-x}Ni_{1+x}O_2$ at high temperatures (and even down to low temperatures for $x = 0.02$), they also indicate that, in the case of $x = 0.07$, ferro- or ferrimagnetic order sets in below 240 K, at least in some parts of the sample. Indeed, the anomaly observed at this temperature in the χ_{ac} data in the absence of an external magnetic field, together with the rapid increase of this susceptibility with decreasing temperature below 240 K, constitute a first but clear indication for the existence of ferro- or ferrimagnetically ordered regions, especially that the anomaly disappears when an external magnetic field of 2 T is applied. Furthermore, the ESR results provide strong and unambiguous support for the setting-up of such an order below 240 K, as judged from the behavior with decreasing temperature of the two features which appear in the spectra of Figure 4 below 250 K on either side of the main resonance signal. The appearance of these two features may be better understood if we consider the relationship between the spin precession frequency and the applied magnetic field in the case of a ferromagnet. In fact, for a paramagnet, the precession frequency, ω, is directly proportional to the applied magnetic field, H, ($\omega = \gamma H$), where γ is the gyromagnetic ratio. However, for a ferromagnet, the internal field has to be taken into account in addition to the applied field, implying that the frequency-field relationship, not only will it be different from the paramagnetic case, but will also depend on whether or not the applied field is along the direction of the easy axis of magnetization. If the applied field is parallel to the easy-axis direction, the linear relationship between ω and H will hold but only beyond a threshold frequency, ω_0, since, in that case, $\omega = \omega_{\parallel} = \omega_0 + \gamma H$, where ω_0 is a frequency gap associated with a critical field H_c representing the magnetic anisotropy ($\omega_0 = \gamma H_c$). On the other hand, if the applied field is perpendicular to the easy-axis direction, two regimes are distinguished in the frequency-field diagram: i) for $0 \leq H \leq H_c$, ω is given by

$$\omega = \omega_{\perp} = \gamma H_c \sqrt{1 - \left(\frac{H}{H_c}\right)^2} \tag{1}$$

ii) for $H \geq H_c$, ω is given by

$$\omega = \omega_{\perp} = \gamma H_c \sqrt{H\,(H - H_c)}. \tag{2}$$

These variations of $\omega_{\parallel}$ and $\omega_{\perp}$ with applied magnetic field H are shown schematically in Figure 9. Spin resonance is observed at the field values for which ω is equal to the source frequency, $\omega_r = 2\pi\nu$, where ν is, in our case, 9.45 GHz, as mentioned in Section 2.

When the temperature decreases, the critical field H_c representing the magnetic anisotropy, and, consequently, the frequency gap ω_0, both increase in a manner reflecting the increase of magnetization with decreasing temperature. Therefore, if we were to compare the $\omega_{\parallel}$ - and $\omega_{\perp}$ - *versus* H curves at two different temperatures, T_1 and T_2, (with, say, $T_2 < T_1$), the resonance field value at T_2 would be lower than that at T_1 when the applied field is along the easy-axis direction, and higher if the field is perpendicular to the easy-axis direction.

This above description would of course apply in the case of a ferromagnetic single crystal where an easy-axis direction may be well-defined. However, in this work, we are studying powder polycrystalline samples. In this case, in the ferromagnetic phase, the diagram of Figure 9 would not be restricted to either of the extreme cases represented by the $\omega_{\parallel}$ and $\omega_{\perp}$ curves: it would, instead, show a multitude of intermediary curves reflecting the various possible orientations of the easy axes with respect to the applied magnetic field. Nevertheless, the density of these curves

would be largely concentrated on the two extreme cases represented by the $\omega_{\parallel}$ and $\omega_{\perp}$ curves of Figure 9. As a consequence, two resonance signals would be observed at two different field values: the lower resonance field, H', would decrease as the temperature decreases, while the value of the higher resonance field, H'', would increase.

Following this analysis, we therefore think that the temperature behavior of the two signals observed below 250 K in the spectra of Figure 4 on either side of the central signal, reflects indeed the presence of ferro- or ferrimagnetically ordered regions in the sample below this temperature. It must be noted, however, that the continued presence of the central signal in the spectra throughout the temperature range studied indicates that the main part of the sample is still paramagnetic. The slightly different g-factor corresponding to this central signal, as compared with that for the sample with $x = 0.02$ (see Sect. 3.1 above), is not surprising if we take into account the presence of the ferro- or ferrimagnetically-ordered regions mentioned above.

We now come to the possible origin of such ordered regions. It is well-known that the Ni ions in stoichiometric $LiNiO_2$ are in the Ni^{3+} (spin-1/2) state and that, when excess nickel ions are present in the Li layers, these excess nickel ions are in the Ni^{2+} (spin-1) state [1]. Therefore, in order for charge equilibrium to be respected in the surrounding of each Ni^{2+} ion replacing an Li^+ ion, it is generally assumed that one of the neighboring nickel ions in the nickel layers reverts to the Ni^{2+} state.

The presence of an Ni^{2+} ion in the lithium layers means that magnetic correlations across the layers would now be possible, between this Ni^{2+} ion and its six nearest neighbors in the adjacent nickel layers (see Fig. 1b). Therefore, the immediate environment around such an extra nickel ion may be thought of as a magnetic entity, or cluster, made up of seven nickel ions, two of which being Ni^{2+} (the central one, lying in the lithium layers, and one of its nearest nickel neighbors), while the other five would be the remaining nearest Ni^{3+} neighbors. For the samples having very low concentrations of extra nickel ions (such as in the sample with $x = 0.02$), numerical simulations [27] indicate that only clusters of 7, 12 or 13 nickel atoms are the most likely to exist, with the 7-atom clusters being largely predominant. Therefore, in the sample with $x = 0.02$, such clusters are diluted in the $LiNiO_2$ matrix. In that case, we would expect a paramagnetic behavior down to low temperatures, as is clear from the ESR and susceptibility results on $Li_{0.98}Ni_{1.02}O_2$. For $x = 0.07$, the numerical simulations indicate a continued predominance of the 7-atom clusters. Percolation between clusters does not occur as long as x is below 0.136 (see Mertz *et al.* [28]). For $x > 0.136$, the possibility of having a percolation path means that bulk ferrimagnetic order sets in below a certain temperature, T_c, which increases with x up to $T_c \simeq 240$ K for $x = 0.25$ and saturates at this temperature [1,21] for $0.25 \leq x \leq 0.36$. Coming back to the case of our sample with $x = 0.07$, the ferrimagnetic order, which is evident in the ESR spectra of Figure 4 below 250 K as well as in the susceptibility data of Figure 5, must therefore mean that, although the major part of the sample has a concentration of extra nickel ions close to 0.07, clusters containing a macroscopically large amount of Ni atoms exist in some parts of the sample, such that, locally, we would have Ni-rich regions in which the effective x value would be equal to or greater than 0.25. This would explain, on the one hand, the setting up of ferrimagnetic order in these regions below 240 K and, on the other hand, the hypothesis of the existence of two different phases already suggested earlier in this paper from the ESR and the X-ray results. Indeed, confirmation of this hypothesis comes from the Rietveld refinement which we have carried out on the X-ray data, using the Fullprof program [29] and assuming the presence of two phases in the compound. The main phase was supposed to belong to the $R\bar{3}m$ space group, while for the secondary phase, several space groups have been tried among those reported for the $Li_{1-x}Ni_{1+x}O_2$ system. Different starting models have been tested and all of them converged towards the same solution, namely, a mixture of two phases belonging to the $R\bar{3}m$ space group and whose parameters are reported in Table 1. A relatively good agreement is observed between independent variables such as cell parameters, extra-Ni (3b)-site occupancy and results previously reported in the literature. Owing to the uncertainties inherent to the experimental method used, some precautions have to be taken concerning the precision of the obtained values for cell parameters and the percentage of nickel cations on the (3b) site. For instance, the cell parameters and the site occupancies are very sensitive to the half-width parameters U, V and W used in the refinement procedure. Nevertheless, this result seems to confirm unambiguously the existence of a secondary phase present in the sample, with a relatively high concentration of extra nickel atoms.

5 Conclusion

In this work, we have presented X-ray powder diffraction, ESR and ac-susceptibility results on $Li_{1-x}Ni_{1+x}O_2$ samples with $x = 0.02$ and $x = 0.07$. The ESR and ac-susceptibility measurements have been carried out as a function of temperature, between 100 K and room temperature. We have shown that, while the susceptibility of both compounds followed a Curie-Weiss law at high temperatures (with a Weiss temperature, θ, of $\sim$ 30 K for $x = 0.02$ and $\sim$ 80 K for $x = 0.07$), the sample with $x = 0.07$ revealed, in addition, the existence of a ferrimagnetic order setting up below 240 K. These results, together with the X-ray diffraction data, lead us to propose that this ferrimagnetic order is not an intrinsic phenomenon as has been suggested in the literature, but is rather related to the presence of locally Ni-rich regions.

On the other hand, the absence of anisotropy in the ESR spectra of the $Li_{0.98}Ni_{1.02}O_2$ sample deserves a small comment. We think that it is related to the dynamic Jahn-Teller effect that is known to exist in this compound [13,25]. It should be interesting to study this compound at low temperatures and high fields in order to

Table 1. Results of Rietveld refinement for $Li_{1-x}Ni_{1+x}O_2$ with $x = 0.02$ and $x = 0.07$.

$Li_{1-x}Ni_{1+x}O_2$ with $x = 0.07$					
Phase 1					
$a = 0.28820$ nm			Constraints:	Occ(Li) + Occ(Ni_1) = 1	
$c = 1.42131$ nm					
Atoms		Wyckoff Positions		B(Å^2)	Occupancy
Li (3b)	0.00000	0.00000	0.50000	0.660(0)	0.98(1)
Ni_1 (3b)	0.00000	0.00000	0.50000	0.454(9)	0.02(1)
Ni_2 (3a)	0.00000	0.00000	0.00000	0.455(9)	1.00
O (6c)	0.00000	0.00000	0.25846(12)	0.719(20)	2.00
Phase 2					
$a = 0.2888$ nm			Constraints:	Occ(Li) + Occ(Ni_1) = 1	
$c = 1.4221$ nm					
Atoms		Wyckoff Positions		B(Å^2)	Occupancy
Li (3b)	0.00000	0.00000	0.50000	0.660(0)	0.81(3)
Ni_1 (3b)	0.00000	0.00000	0.50000	0.454(9)	0.19(3)
Ni_2 (3a)	0.00000	0.00000	0.00000	0.455(9)	1.00
O (6c)	0.00000	0.00000	0.25781(39)	0.719(20)	2.00
Conventional Rietveld Reliability Factors: $R_p = 6.19$ $R_{wp} = 9.17$ $R_{exp} = 6.49$ $\chi^2 = 2$.					
Phase 1: Bragg R_B-factor = 2.05. Phase 2: Bragg R_B-factor = 4.53					

$Li_{1-x}Ni_{1+x}O_2$ with $x = 0.02$					
$a = 0.2774(1)$ nm			Constraints:	Occ(Li) + Occ(Ni_1) = 1	
$c = 1.4196(1)$ nm				B(Ni_1) = B(Ni_2)	
Atoms		Wyckoff Positions		B(Å^2)	Occupancy
Li (3b)	0.00000	0.00000	0.50000	0.660	0.989(3)
Ni_1 (3b)	0.00000	0.00000	0.50000	0.385(38)	0.011(3)
Ni_2 (3a)	0.00000	0.00000	0.00000	0.385(38)	1.00
O (6c)	0.00000	0.00000	0.25758(30)	0.661(84)	2.00
Conventional Rietveld Reliability Factors: $R_p = 6.15$ $R_{wp} = 10.1$ $R_{exp} = 6.27$ $\chi^2 = 2.59$.					
Phase 1: Bragg R_B-factor = 2.01					

$R_p = 100 \times \Sigma(Y_{obs} - Y_{calc})/\Sigma Y_{obs}$; $R_{wp} = 100 \times [\Sigma w(Y_{obs} - Y_{calc})^2/\Sigma Y_{obs}^2]^{1/2}$; $R_{exp} = 100 \times [(N-P)/\Sigma(wY_{obs}^2)]^{1/2}$; $R_B = 100 \times \Sigma(I_{obs} - I_{calc})/\Sigma I_{obs}$; Y_{obs},Y_{calc}: observed and calculated intensities; I_{obs}, I_{calc}: observed and calculated integrated intensities; w: weight allocated to each data point; N: number of profile points; P: number of parameters.

check if a static Jahn-Teller distorted structure may then be stabilized.

References

1. J.B. Goodenough, D.G. Wickham, W.J. Croft, J. Phys. Chem. Sol. **5**, 107 (1958).
2. J.N. Reimers, J.R. Dahn, J.E. Greedan, C.V. Stager, G. Liu, I. Davidson, U. von Sacken, J. Sol. St. Chem. **102**, 542 (1993).
3. C. Delmas, *Chemical Physics of Intercalation* (Plenum Press, New York, 1988) p. 209.
4. J.R. Dahn, U. von Sacken, C.A. Michal, Sol. St. Ionics **44**, 87 (1990).
5. R. Kanno, H. Kubo, Y. Kawamoto, T. Kamiyama, F. Izumi, Y. Takeda, M. Takano, J. Sol. St. Chem. **110**, 216 (1994).
6. H. Arai, S. Okada, H. Ohtsuka, M. Ichimura, J. Yamaki, Sol. St. Ionics **80**, 261 (1995).
7. K. Hirakawa, H. Kadowaki, K. Ubukoshi, J. Phys. Soc. Jpn **54**, 3526 (1985).

8. I. Yamada, K. Ubukoshi, K. Hirakawa, J. Phys. Soc. Jpn **54**, 3571 (1985).
9. I. Yamada, K. Ubukoshi, K. Hirakawa, J. Phys. Soc. Jpn **55**, 3689 (1986).
10. M. Itoh, I. Yamada, K. Ubukoshi, K. Hirakawa, H. Yasuoka, J. Phys. Soc. Jpn **55**, 2125 (1986).
11. K. Hirakawa, R. Osborn, A.D. Taylor, K. Takeda, J. Phys. Soc. Jpn **59**, 3081 (1990).
12. J.P. Kemp, P.A. Cox, J.W. Hodby, J. Phys.-Cond. Matter **2**, 6699 (1990).
13. R. Stoyanova, E. Zhecheva, C. Friebel, J. Phys. Chem. Sol. **54**, 9 (1993).
14. P. Ganguly, V. Ramaswamy, I.S. Mulla, R.F. Shinde, P.P. Bakare, S. Ganapathy, P.R. Rajamohanan, N.V.K. Prakash, Phys. Rev. B **46**, 11595 (1992).
15. C.B. Azzoni, A. Paleari, V. Massarotti, M. Bini, D. Capsoni, Phys. Rev. B **53**, 703 (1996).
16. C.B. Azzoni, A. Paleari, V. Massarotti, D. Capsoni, J. Phys.-Cond. Matter **8**, 7339 (1996).
17. M. Rosenberg, P. Stelmaszyk, V. Klein, S. Kemmler-Sack, G. Filoti, J. Appl. Phys. **75**, 6813 (1994).
18. M. Corti, S. Marini, A. Rigamonti, V. Massarotti, D. Capsoni, J. Appl. Phys. **79**, 6621 (1996).
19. K. Yamaura, M. Takano, A. Hirano, R. Kanno, J. Sol. St. Chem. **127**, 109 (1996).
20. A. Bajpai, A. Banerjee, Phys. Rev. B **55**, 12439 (1997).
21. A. Rougier, C. Delmas, G. Chouteau, J. Phys. Chem. Sol. **57**, 1101 (1996).
22. K. Hirota, Y. Nakazawa, M. Ishikawa, J. Magn. Magn. Mater. **90-91**, 279 (1990).
23. K. Hirota, Y. Nakazawa, M. Ishikawa, J. Phys.-Cond. Matter **3**, 4721 (1991).
24. H. Yoshizawa, H. Mori, K. Hirota, M. Ishikawa, J. Phys. Soc. Jpn **59**, 2631 (1990).
25. A.-L. Barra, G. Chouteau, A. Stepanov, C. Delmas, J. Magn. Magn. Mat. **177-181**, 783 (1998).
26. A. Rougier, P. Gravereau, C. Delmas, J. Electrochem. Soc. **14**, 1168 (1996).
27. D. Mertz, DEA report: *Magnétisme de* $Li_{1-x}Ni_{1+x}O_2$. *Modélisation et simulation numérique* (Université de Provence, 1998).
28. D. Mertz, Y. Ksari, F. Celestini, J.-M. Debierre, A. Stepanov, C. Delmas, Phys. Rev. B **61**, 1240 (2000).
29. J. Rodriguez-Carvajal, *FULLPROF: a Program for Rietveld Refinement and Pattern Matching Analysis. Abstract of the Satellite Meeting on Powder Diffraction of the XVth Congress of the International Union of Crystallography* (Bordeaux, 1990) p. 127.